Hyperspectral Imaging System Calibration using Image Translations and Fourier Transform

Nathalie Gorretta, Gilles Rabatel, Christophe Fiorio, Jean-Michel Roger, Camille Lelong, Véronique Bellon Maurel

Author-produced version of the article published inJournal of Near Infrared Spectroscopy, 2008, 16, 4, 371-380.
The original publication is available at http://www.impublications.com/
doi: 10.1255/jnirs.809

Hyperspectral Imaging System Calibration using image translations and Fourier Transform - Version 06

Gorretta, N.[a], Rabatel, G. [a],Roger, J.M.[a], Fiorio, C.[b], Lelong, C. [c], Bellon-Maurel, V.[a]

a - Cemagref, UMR ITAP Montpellier FRANCE

b - Laboratoire d'Informatique, de Robotique et Microélectronique, Montpellier FRANCE

c - CIRAD, UMR TETIS, Montpellier FRANCE

25 juin 2010

Résumé

In this paper, we describe a methodology based on imaging system shifting and Fourier transform to recover the spatial distribution of the sensivity of an hyperspectral imaging system. The methodology mainly adresses hyperspectral imaging system based on a CCD sensor for proximity image acquisition. The principle is to look several times at the same scene by moving slightly the camera at each acquisition. Thus, it is possible to separate what moves (scene) from what remains fixed (response of the system) using properties of Fourier Transform. Tests on synthetic images has reinforced theorical results on contraints shifts and gives good results with more than ten translations.Tests on real and in-lab images have shown the need of accurate determination of translation to avoid some disruptive effects (pattern multiplication). Nevertheless, the results are promising and have shown the potentialities of the methodology to correct images from spatial non-uniformity due to the imaging system. We notice that such a methodology remains valid for any imaging system based on a CCD sensor.

1 Introduction

Calibrating imaging system response is necessary because image acquisition systems are not perfect and the resulting images are degraded version of reality. Degradation factors are various : geometric and radiometric aberrations due to the sensor and the optics, perturbations due to external conditions (e.g, atmospheric perturbations in remote sensing applications), noise (i.e, thermic, readout, shot and random noise). A lot of algorithms used in computer vision require precise measurements of scene radiance to recover scene properties (Grossberg and Nayar, 2002). Indeed, authors have proposed some calibration methods to charaterize both temporal and systematic noises and/or to estimate the radiometric response from the imaging system. Some of them use, for exemple, a full range of known radiance values (e.g. Macbeth Chart) other estimate directly the response function of the imaging device (Healey, 1994),(Tarel, 1995), (Tsin et al., 2001), (Wonpil et al., 2004).

Hyperspectral imaging corresponds to the fusion of imaging and spectroscopy. It produces intensity images over a continuous range of narrow spectral bands. Even more than standard imaging systems, hyperspectral platforms require accurate calibration to provide reliable and reproductible measurements (Polder and Van Der Heijden, 2001). The calibration process includes wavelength calibration and detector nonuniformity correction, sensor artifacts and backgrounds levels. Few authors propose calibration methods to calibrate hyperspectral imaging where the imaged object is close to the imaging system (proximity imaging system). Polder (Polder et al., 2003) describes methods to accurately characterize a spectrograph-based spectral imaging system investigating the impact of various sources of noise, the signal ratio per wavelength and the spectral and spatial resolution of the system. Lawrence (Lawrence et al., 2003) proposes a method to calibrate a pushbroom hyperspectral imaging system for spatial dimensions, spectral wavelength and percent reflectance value. Mansouri (Mansouri et al., 2005) proposes a protocole for a multispectral imaging system based on CCD sensor measuring the systematic error using

a model developed by Healey (Healey, 1994). However, most of the users using laboratory hyperspectral imaging systems only perform a radiometric calibration using the one point calibration method (Geladi et al., 2004), (Lawrence et al., 2003), (Lyon et al., 2002). This method deals with the acquisition of a flat image obtained on a reference standard close to 100% reflectance, and subtraction of the dark current. However, the calibration results includes the illumination heterogeneities and is thus efficient in a stabilized environnement where the illumination variations are limited by an adapted instrumentation or/and by a periodic calibration (laboratory, or industrial applications). This method is however not usable when the camera has to be used in various locations and lighting conditions (e.g outdoors image acquisition).

To face these drawbacks, we propose a method allowing to separate non uniformities due to the scene from the ones due to the acquisition system. The principle is to acquire several images of the same scene while moving slightly the camera at each time. Thus, it is possible to separate what moves (scene) from what remains unchanged (response of the system). The Fourier transform allows to formalize camera translations in a linear form and thus allows us to obtain a simple solution.

In the first section, we describe the theoretical bases of our approach : imaging system modelling and Fourier transform to determine the imaging system response. The second section illustrates the proposed approach on synthetic images and on real hyperspectral images.

2 Basic principles

2.1 System modelisation

Let (x, y) be the spatial coordinates in the sensor plane and λ the wavelength. Let us consider an hyperspectral imaging system depicted in figure 1. We denote the spectral radiance of the object surface imaged in a pixel (x, y) by $L(\lambda, x, y)$, the spectral transmit-

tance of the optical system $O(\lambda)$ including lens and filters and the spectral sensitivity of the pixel (x, y) by $S(\lambda, x, y)$.

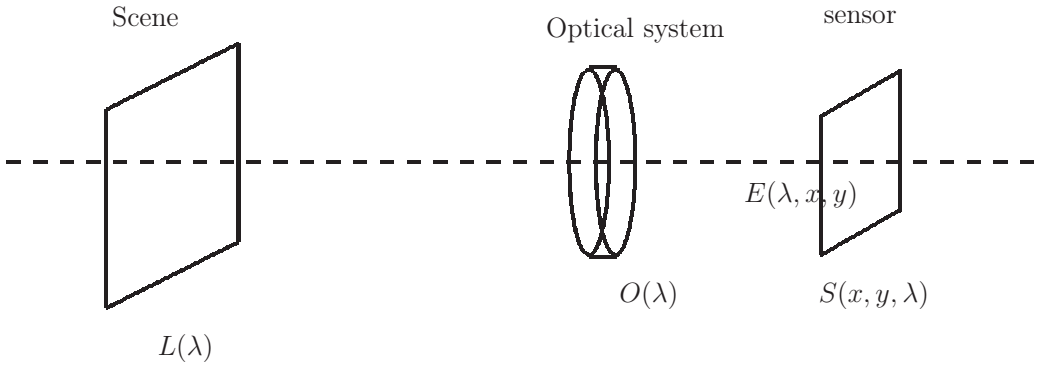

FIG. 1 – Imaging system

Assuming this system has an ideal Point Spread Function or PSF (i.e. a point in a scene corresponds to a unique pixel in the image) and using the single lens model proposed by Horn (Horn, 1986), we assume that the irradiance $E(\lambda, x, y)$ on the element (x, y) of the image sensor is proportional to the spectral scene radiance $L(\lambda, x, y)$:

$$E(\lambda, x, y) = L_(\lambda, x, y) \cdot O(\lambda) \tag{1}$$

The term $O(\lambda)$ comprise several complex factors such as vignetting (filter and lens) and lens fall-off (lens).

Supposing a linear radiometric response of the imaging sensor, the corresponding brightness $I(\lambda, x, y)$ of the pixel (x, y) is then given by equation 2 :

$$I(x, y, \lambda) = L_(\lambda, x, y) \cdot O(\lambda) \cdot S(x, y, \lambda) \tag{2}$$

Regardless of the individual factors involved, we can assume that the mapping from scene radiance to the image brightness is a multiplication of two functions $L(\lambda, x, y)$ and

$V(\lambda, x, y)$:

$$I(x, y, \lambda) = L(\lambda, x, y) \cdot V(\lambda, x, y)$$
$$\text{with } V(\lambda, x, y) = O(\lambda) \cdot S(x, y, \lambda) \quad (3)$$

The term $V(\lambda, x, y)$ models the process by which the spectral radiance of a scene point is converted to a pixel brightness by the imaging system.

The aim of the proposed method is to recover this latter function. Because it only depends on the imaging system, it will be reusable in any image grabbing configuration.

2.2 Determination of $V(\lambda, x, y)$ by imaging system shifting

Given the wavelength λ, equation 3 becomes $I(x, y) = L(x, y) \times V(x, y)$.

If the optical system is slightly translated with a translation vector $\vec{T_0}$, the brightness of the pixel (x, y) is now proportional to the radiance of the corresponding point scene $(x + t_x, y + t_y)$, where (t_x, t_y) is the equivalent in the image of the translation $\vec{T_0}$ $(t_x, t_y) = -G \cdot \vec{T_0}$ (with G equal to magnification). However, the term $V(x, y)$ will remain unchanged. The translated image I_t due to the translation vector $\vec{T}$ (t_x, t_y), is then written :

$$I_t(x, y) = L((x - t_x, y - t_y) \cdot V(x, y)$$

Let us consider the logarithm of the original image $I(x, y)$ (equation 4) and the translated image $I_t(x, y)$ (equation 5) :

$$\begin{aligned} \log(I(x, y)) &= \log(L(x, y)) + \log(V(x, y)) \\ &= a_0(x, y) + b(x, y) \end{aligned} \quad (4)$$

$$\begin{aligned} \log(I_t(x,y)) &= \log(L(x-t_x, y-t_y)) + \log(V(x,y)) \\ &= a_0(x-t_x, y-t_y) + b(x,y) \end{aligned} \tag{5}$$

The Fourier transform is then applied to the equations 4 and 5. The Fourier transform of term $b(x,y)$ noted $\mathfrak{F}(b(x,y))$ is $B(u,v)$, u and v being frequency domain variables.

The translation acts on the Fourier spectrum as a phase shift but the magnitude of the spectrum remains unchanged. More precisely, in the Fourier space, the translation yields a multiplication of $\mathfrak{F}(a_0(x,y)) = A_0(u,v)$ by a term $K = e^{-2j\pi(t_x.u+t_y.v)}$. Thus, setting $\mathfrak{F}(log(I(x,y))) = X(u,v)$ and $\mathfrak{F}(log(I(x-t_x, y-t_y))) = X_t(u,v)$, the Fourier transforms of equations 4 et 5 can be written respectively :

$$X(u,v) = \mathfrak{F}(a_0(x,y)) + \mathfrak{F}(b(x,y)) = A_0(u,v) + B(u,v) \tag{6}$$

$$X_t(u,v) = \mathfrak{F}(a_0(x-t_x, y-t_y)) + \mathfrak{F}(b(x,y)) = A_0(u,v) \cdot K + B(u,v) \tag{7}$$

By using equations 6 and 7, we are able to recover $A(u,v)$ and $B(u,v)$ (equations 8 and 9) and next the terms $V(x,y)$ and $L(x,y)$ by reverse transformations (equations 10 and 11) :

$$A_0(u,v) = \frac{X(u,v) - X_t(u,v)}{1-K} \tag{8}$$

$$B(u,v) = X(u,v) - A_0(u,v) \tag{9}$$

$$L(x,y) = \exp(\mathfrak{F}^{-1}(A_0(u,v))) \tag{10}$$

$$V(x,y) = \exp(\mathfrak{F}^{-1}(B(u,v))) \tag{11}$$

The term $1 - K = 1 - exp^{j\alpha(u,v)}$ is susceptible to be equal to zero for some values of (u,v), yielding an indetermination of $A(u,v) = \frac{X_t(u,v) - X(u,v)}{1-K}$. Two cases can be distinguished :

1. $(u,v) = 0$ and so $K = e^0 = 1$. Spectral components $(u = 0, v = 0)$ correspond to the average value of $log(L(x,y))$. It means that the average value of $L(x,y)$ cannot be obtained. This case of indetermination illlustrates that the proposed method can only determine the term $L(x,y)$ with respect to the function $V(x,y)$ with a multiplying factor. The same scene with a double lighting intensity, combined with a doubled radiometric attenuation through the term $V(x,y)$, would lead to the same image.

2. $K = e^{2jp\pi}$ i.e, $T_x \cdot u + T_y \cdot v = p$ with $p \in \aleph^+$

   The values (u,v) giving these indeterminations concern a network of parallel straight lines, perpendicular to the translation $\overrightarrow{T}$ (figure 2 a, b and c). It means that it is not possible to determine the frequential components of function $L(x,y)$ with a period equal to a whole division of the translation $\overrightarrow{T}$ (harmonics). Indeed, if such frequential components are present in the image it is not possible to determine if they move with the translation or not.

2.3 Management of the indetermination cases

2.3.1 $u = 0$ and $v = 0$

To overcome this indetermination case, we impose $\mathfrak{F}(log(L(0,0)) = A(0,0) = \overline{log(I)}$, i.e, we impose the term $\overline{log(L(x,y))}$ to be equal to $\overline{log(I(x,y))}$.

Author-produced version of the article published inJournal of Near Infrared Spectroscopy, 2008, 16, 4, 371-380.
The original publication is available at http://www.impublications.com/
doi: 10.1255/jnirs.809

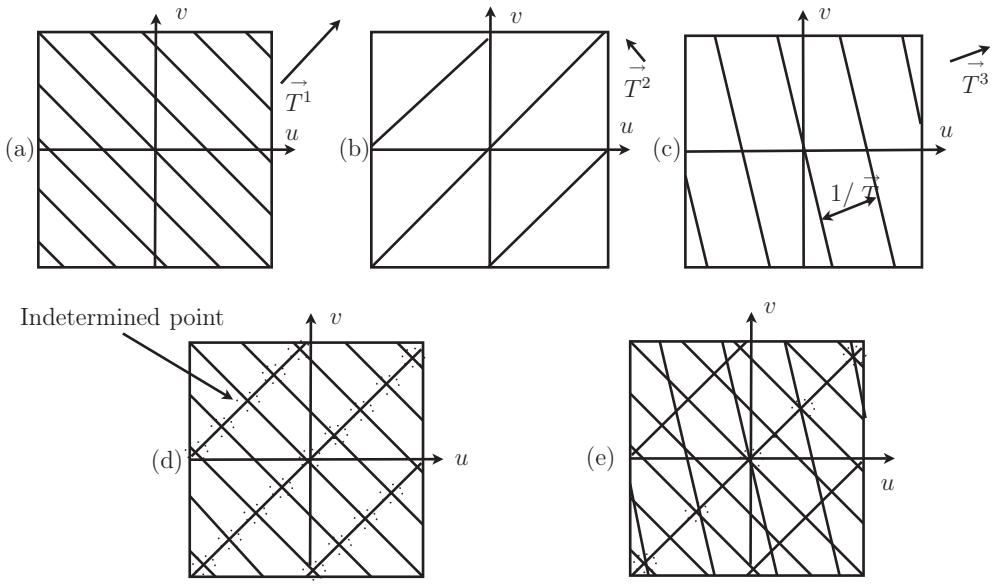

FIG. 2 –
(a), (b) and (c) indetermination cases due to translations $\vec{T}^1$, $\vec{T}^2$ and $\vec{T}^3$ respectively
(d) Remaining indetermination cases with translation combination $\vec{T}^1$ and $\vec{T}^2$
(e) Remaining indetermination cases with translation combination $\vec{T}^1$, $\vec{T}^2$ and $\vec{T}^3$

2.3.2 $K = e^{2jp\pi}$ i.e, $T_x \cdot u + T_y \cdot v = p$ with $p \in \aleph^+$

A way to reduce the number of indetermination cases consists in carrying out more than one translation. In this case, n images $I_t^1, I_t^2, \cdots, I_t^n$ are acquired with corresponding translations $T^i = (t_x^i, t_y^i)$, with $i = 1 \cdots n$. According to equation 5, we can write for each translated image I_t^i (equation 12) :

$$X_t^i(x, y) = A_0(u, v) \cdot K^i + B(u, v) \tag{12}$$

yielding the system :

$$\begin{aligned} X(u,v) &= A(u,v) + B(u,v) \\ X_t^1(u,v) &= A_0(u,v) \cdot K^1 + B(u,v) \\ X_t^2(u,v) &= A_0(u,v) \cdot K^2 + B(u,v) \\ &\vdots \\ X_t^n(u,v) &= A_0(u,v) \cdot K^n + B(u,v) \end{aligned} \tag{13}$$

and so :

$$\begin{aligned} A_0(u,v) &= \frac{X(u,v) - X_t^1(u,v)}{1 - K^1} \\ A_0(u,v) &= \frac{X(u,v) - X_t^2(u,v)}{1 - K^2} \\ &\vdots \\ A_0(u,v) &= \frac{X(u,v) - X_t^n(u,v)}{1 - K^n} \end{aligned} \tag{14}$$

Finally, the term $A_0(u,v)$ is determined by adding all the numerators and the denominators of the above equations (equation 15) :

$$A_0(u,v) = \frac{\sum_{i=1}^{n} X(u,v) - X^i(u,v)}{\sum_{i=1}^{n}(1 - K^i)} \tag{15}$$

Indeed, each translation gives indetermination cases consisting in a network of parallel straight lines. Several translations combines all these networks : the resulting indetermination cases will be located at the intersections of all the straight lines (figure 2 d and e). For the remaining indetermination cases ($\sum_{i=1}^{n}(1-K^i) = 0$), we impose an arbitrary value to $A_0(u,v)$.

Author-produced version of the article published inJournal of Near Infrared Spectroscopy, 2008, 16, 4, 371-380.
The original publication is available at http://www.impublications.com/
doi: 10.1255/jnirs.809

However, the number, the amplitude and the direction of the translations contribute to the limitation of the indetermination cases :

- An important number of translations involves fewer indetermination cases (figure 2) ;
- Translations must be un-colinear ;
- Translation of limited amplitude give fewer indetermination cases (figure 3) ;

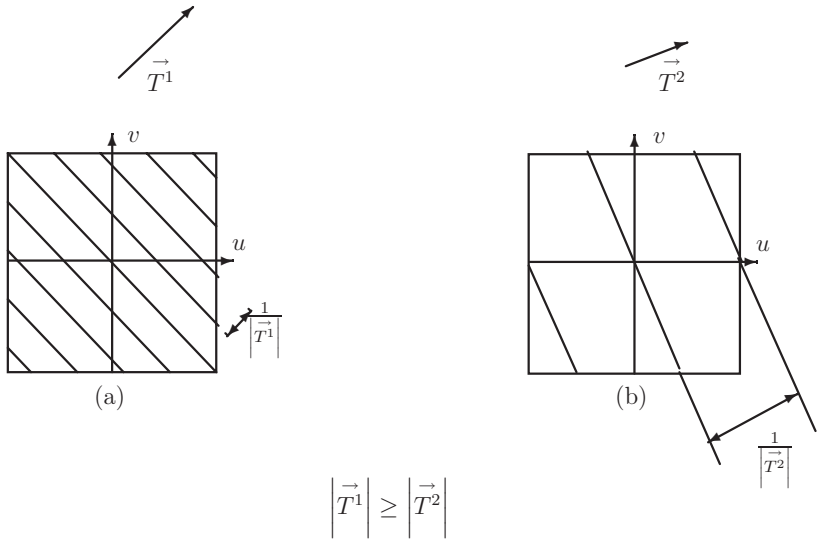

FIG. 3 –(a),(b) indeterminations due to translations $\vec{T^1}$ and $\vec{T^2}$ respectively, with $\left|\vec{T^1}\right| \geq \left|\vec{T^2}\right|$

3 Material and methods

The method was first tested on synthetic images, and then or real images. This chapter describes the building of synthetic images and the acquisition of real images.

3.1 Synthetic images

A gray level image with a 512×512 pixels size and a 8 bit resolution was first acquired (figure 4-a). This original image (I^0) was then used to build the translated images

Author-produced version of the article published inJournal of Near Infrared Spectroscopy, 2008, 16, 4, 371-380.
The original publication is available at http://www.impublications.com/
doi: 10.1255/jnirs.809

$\left\{I^1 \cdots I^n\right\}$. To obtain a good spatial repartition of the translations and to limit the indetermination cases (see chapter 2.3), the amplitude and the direction on each translation vector were determined as follows (equation 17) :

$$\begin{aligned} \vec{T^i} &= \rho^i e^{\Theta^i} \\ \rho^i = \rho^{i-1} \times 1.1 \quad \text{with} \quad i &= 1 \cdots n \\ \Theta^i &= \Theta^{i-1} + \frac{2\pi}{n} \\ \text{with} \quad n \quad &\text{number of translations} \\ \text{Initial conditions :} \rho^1 = 3 \quad &\text{and} \quad \Theta^1 = 0 \end{aligned} \tag{16}$$

To simulate the transformations induced by the imaging system, a Hamming function $g(x, y)$ such as $g(x, y) = \frac{1}{4}(1 - \cos\frac{2\pi x}{512})(1 - \cos\frac{2\pi y}{512})$, where $x = y = 0$ to the image center (figure 4-b) was built.The n images were then combined with $g(x, y)$. An exemple of a resulting image is given figure 4-c.

FIG. 4 – (a)-Original image (left), (b)-Imaging system response (center) (c)-Obtained image (right)

3.2 Real images

3.2.1 Hyperspectral system

Acquisitions were carried out with an hyperspectral imaging system. This system was composed of a diffused light source, a monochrome camera combined with a lens, linked to a variable filter. The apogee monochrome camera was fitted with a 1024*1024 Marconi CCD sensor, enabling a 16-bit digitalization and integration times ranging from 10ms to 10mn. A cooling Peltier system was included in the camera. A Linear Crystable tunable filter or LCTF (Varispec from Cambridge Research and Instrumentation) enabled us to select wavelengths from 650 to 1100 nm, with a spectral resolution of 2,2 nm. The zoom-type-lens (SYGMA) was endowed with a focal varying from 28 to 135 mm. The light source was composed of two non dichroic halogen lamps (OSRAM HALOPOST, 12V-50W) supplied by stabilised power connections. The camera was positioned on a mechanical structure allowing displacement in x and y directions with a step equal to 10 mm (figure 5).

3.2.2 Image acquisition

Ninety one wavelengths between 650 to 1100 nm (every 5 nm) were used. Camera binning in the horizontal and the vertical direction were set to two pixels, giving a 512×512 resolution. The lens opening was set to 16 and the focal at 135mm. For each wavelength, the integration time was computed to prevent camera saturation and to balance the system spectral response. The camera has a wavelenth-dependent dark current, so a dark-current image was recorded for each wavelength ($D(\lambda)$). Acquisitions were performed using a simple white paper sheet on which crosses were drawn to find the translations (see section 3.2.3). The process to acquire the set of images $\left(I^0_{\lambda_1}, I^0_{\lambda_2} \cdots I^0_{\lambda_p}\right)$, $\left(I^1_{\lambda_1}, I^1_{\lambda_2} \cdots I^1_{\lambda_p}\right)$, $\cdots \left(I^n_{\lambda_1}, I^n_{\lambda_2} \cdots I^n_{\lambda_p}\right)$ with $I^j_{\lambda_i}$ image acquired with the translation vector $\overrightarrow{T^j}$ at wavelength λ_i is summarized figure 6.

Following the above-mentionned acquisition process, a set of eight images with uncolinear translation vectors of small amplitude was acquired.

Author-produced version of the article published inJournal of Near Infrared Spectroscopy, 2008, 16, 4, 371-380.
The original publication is available at http://www.impublications.com/
doi: 10.1255/jnirs.809

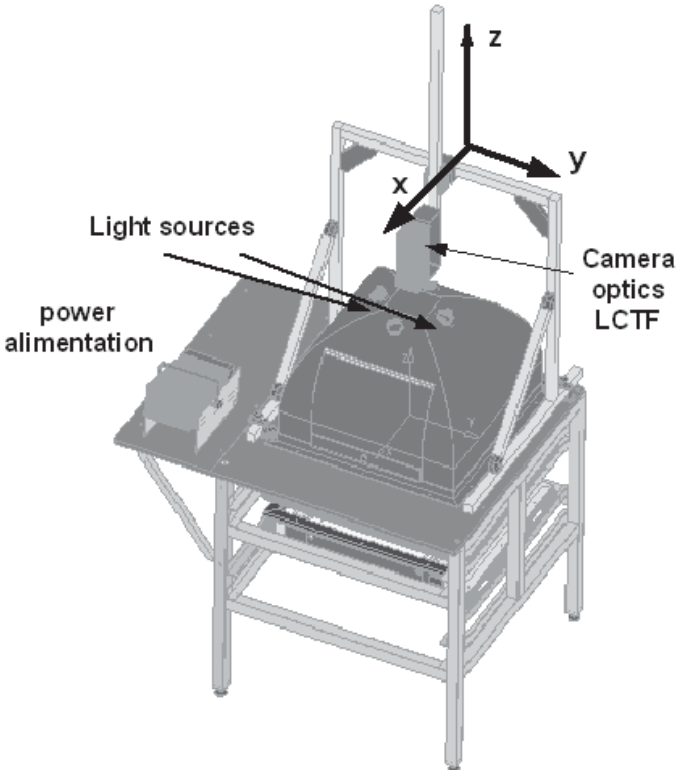

FIG. 5 – Imaging system

3.2.3 Translation determination

The determination of the translation vectors has been achieved using image matching. In this case, the objective was to define a region of interest (ROI) around a reference point in the original image and to find the corresponding region of interest in the translated image. The correlation between the two ROI was assessed by the sum of squared difference or SSD : Let $P^0(x^0, y^0)$ and $P^1(x^1, y^1)$ be respectively the reference point on the original (I^0) and the translated (I^1) image and let $[-n, n]$ be the size of the ROI. Then, the SSD will take the following form :

$$SSD(P^0, P^1) = \sum_{i=-n}^{n} \sum_{j=-n}^{n} \left[\left(I^0(x^0 + i, y^0 + j \right) - \left(I^1(x^1 + i, y^1 + j \right) \right]^2 \qquad (17)$$

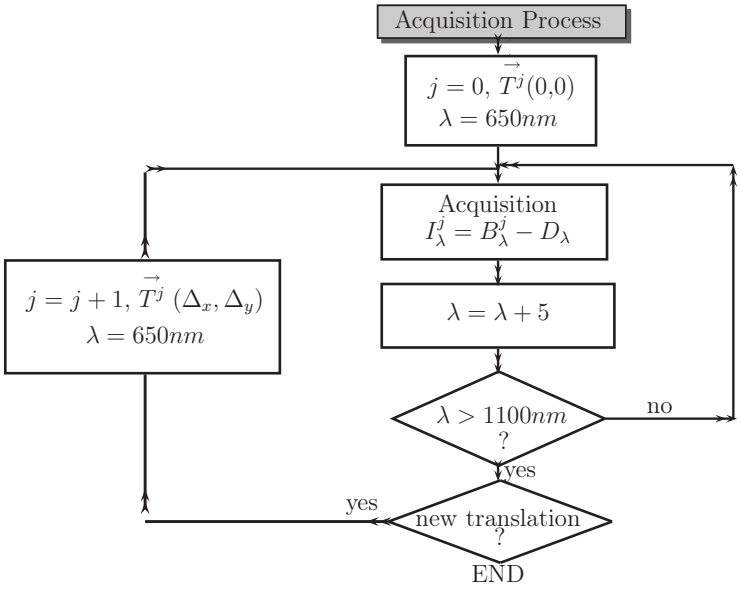

FIG. 6 – Image Acquisition

3.3 Software implementation

The whole software necessary for the proposed method achievement and the data processing was developed in C++ language.

4 Results and discussion

4.1 Synthetic images

The classical measure for images comparison is the cumulative mean squared error or MSE (Van der Weken et al., 2004). The MSE between the corrected image $V^c(x, y)$ and the original one $V(x, y)$) was computed for an increasing number of translations (equation 18). The objective was to determine how many translations are suitable to get correct results.

$$MSE(V(x,y),V^c(x,y)) = \frac{1}{n \times m}\sum_{x=1}^{n}\sum_{y=1}^{m}[V(x,y) - V^c(x,y)]^2$$
$$\text{with :} \quad V(x,y): \quad \text{Original imaging system response}$$
$$V^c(x,y): \quad \text{Calculated imaging system response}$$
$$[n,m]: \quad \text{size of image} \tag{18}$$

The figure 7 shows the evolution of the distance between the obtained and the original imaging system response with an increasing number of translated images. This distance drops consequently up to ten translations. After, ten translations, we can notice a barely noticeable decline. Indeed, to limit the number of transations in real case, ten translations appears as a good compromise. The figure 8 shows the imaging system response recovery obtained using five, ten and twenty translations. Results appear to suffer of large border effects while applying five to ten translations. They look visualy good for twenty images. However, we can observe that the mean gray level of the resulting image appears lower than the original one. Indeed, due to indetermination case ($u = 0$,$v = 0$) (see section 2.3), the mean gray level of the resulting image was set arbitrary as the mean gray level of the original image. This setting value induces a gray level shift on the corrected image.

4.2 Real images

By considering that the response of the system is dependent of the selected wavelength, experimentations was carried out on each of them. Indeed, for a complete standardization of the imaging system, a stardardization image was obtained and applied for each wavelength. Figure 9 shows the imaging system response $V(x,y)$ obtained for several wavelength (650, 800, 1000 nm). Figure 10 shows the evolution of the imaging system response over sensor spectral range for a sensor line (x=256).

Author-produced version of the article published inJournal of Near Infrared Spectroscopy, 2008, 16, 4, 371-380.
The original publication is available at http://www.impublications.com/
doi: 10.1255/jnirs.809

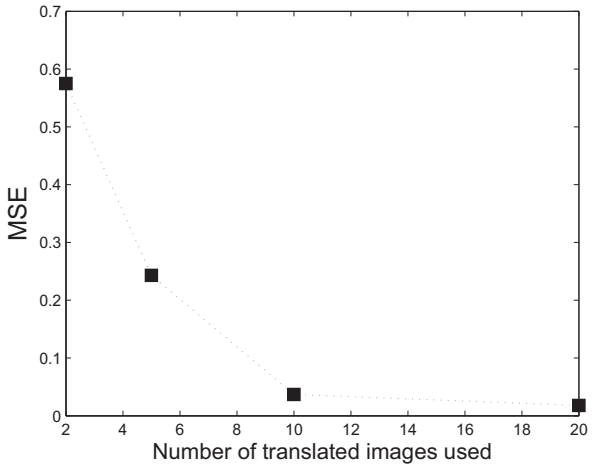

FIG. 7 – MSE evolution with an increasing number of translated images

original images – 5 translations – – 10 translations – – 20 translations –

FIG. 8 – Results obtained on synthetics images and with five, ten and twenty translated images (scene image up and imaging system response down)

Author-produced version of the article published inJournal of Near Infrared Spectroscopy, 2008, 16, 4, 371-380.
The original publication is available at http://www.impublications.com/
doi: 10.1255/jnirs.809

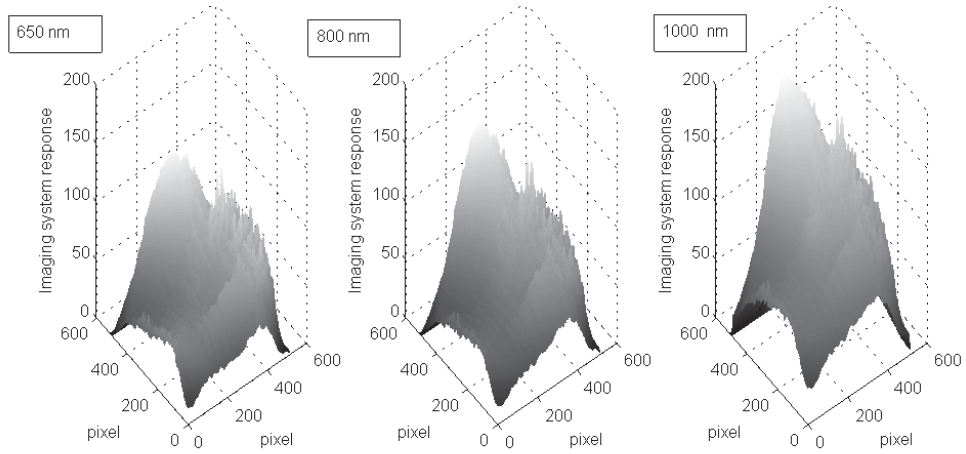

FIG. 9 – Imaging system response (V(x,y)) for three wavelength : 650 nm (left), 800 nm (center), 1000 nm (right)

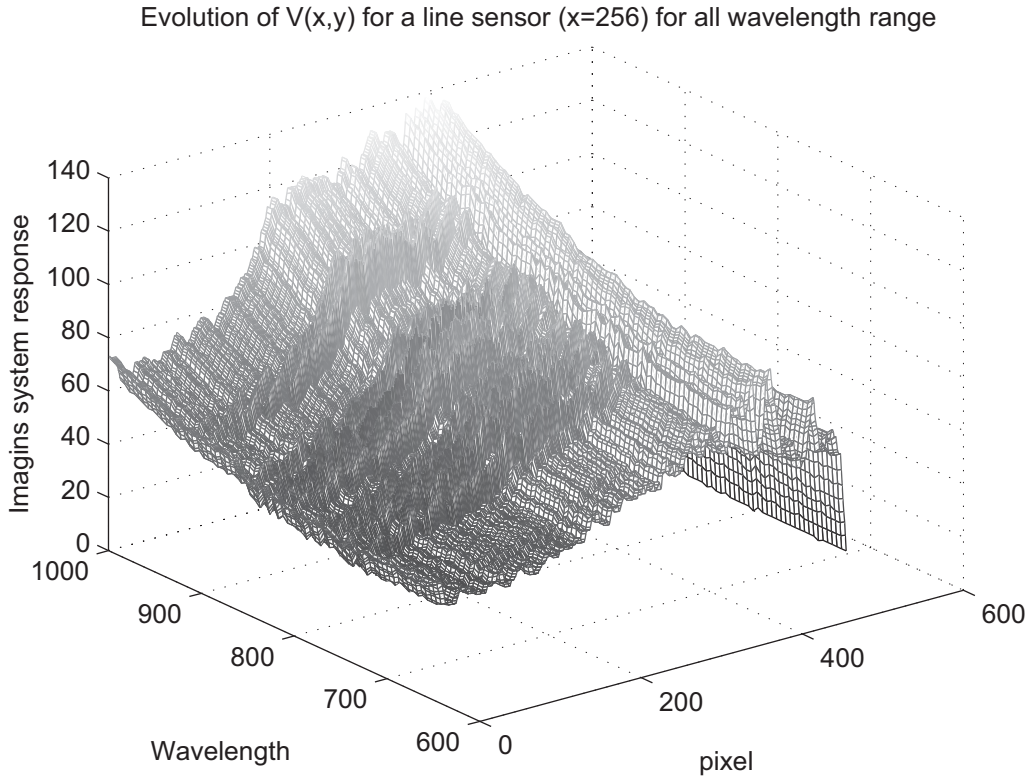

FIG. 10 – Imaging system response as a function of wavelength for a line sensor (x=256)

Author-produced version of the article published inJournal of Near Infrared Spectroscopy, 2008, 16, 4, 371-380.
The original publication is available at http://www.impublications.com/
doi: 10.1255/jnirs.809

However, for easiness of reading, the results presented below are detailed for only one wavelength i.e. $650nm$. The Figure 11 and 12 show respectively the amplitude and direction of used translation vector and the resulting acquired images at the wavelength 650 nm (I^0_{650nm}, I^1_{650nm}, I^2_{650nm}, $\cdots$, I^7_{650nm}, I^8_{650nm},.

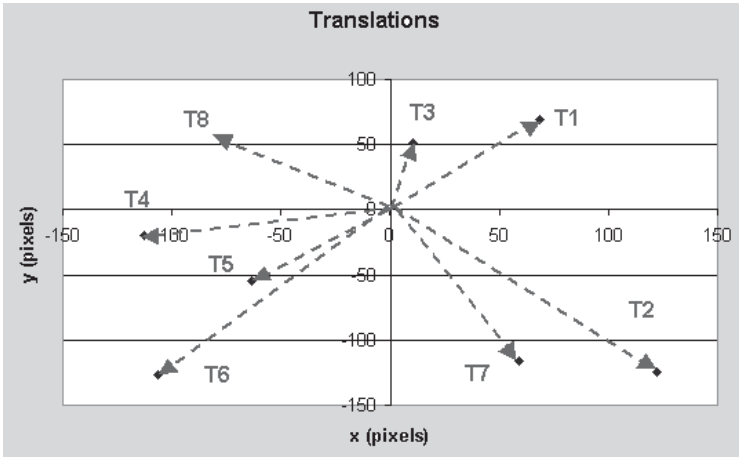

FIG. 11 – Translation Vectors (**E**xperiment 3)

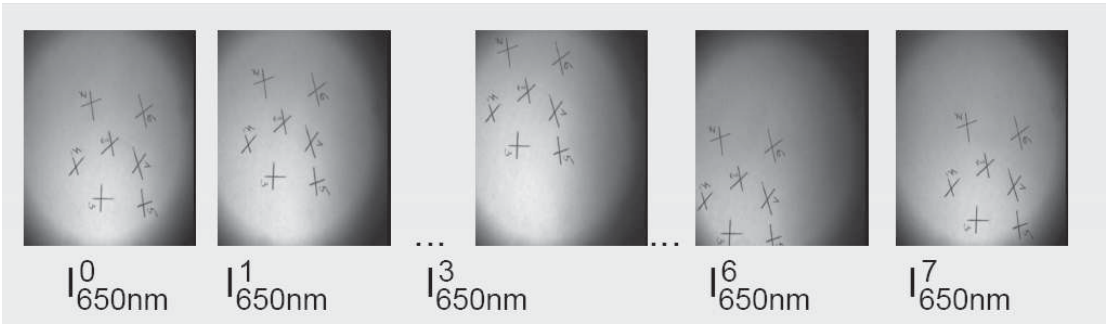

FIG. 12 – Acquired images I^0_{650nm}, I^1_{650nm}, I^2_{650nm}, $\cdots I^7_{650nm}$, I^8_{650nm} (**Experiment 3**)

As said above, two main problems occurs either if the number of translation is to small or if translations are colinear. They are described in the following examples. Figure 13 shows the function $L(x, y)$ and $V(x, y)$ obtained with only one translation vector (T_1). The results are consistent with the theory exposed in section 2.2, i.e obtained images are stripped with a periodic pattern. Indeed, using only one translation does not allow to separate $L(x, y)$ from $V(x, y)$ functions in a direction perpendicular to the translation.

Figure 14 shows $L(x, y)$ and $V(x, y)$ functions obtained with four translated images with colinear translation vectors. The lines generated by the indetermination cases ($\sum(1 - K_i) = 0$) are almost parallels because their combinations are not sufficient. Thus, results display waves features related to dominant indetermination axis.

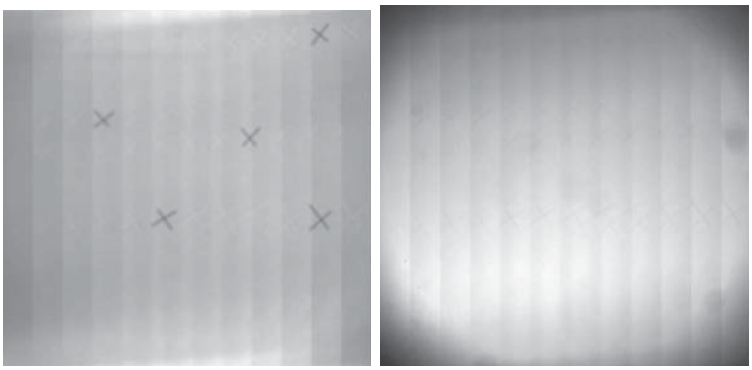

FIG. 13 – Results obtained with real images using only one translated image : L(x,y) (left), V(x,y) (right)

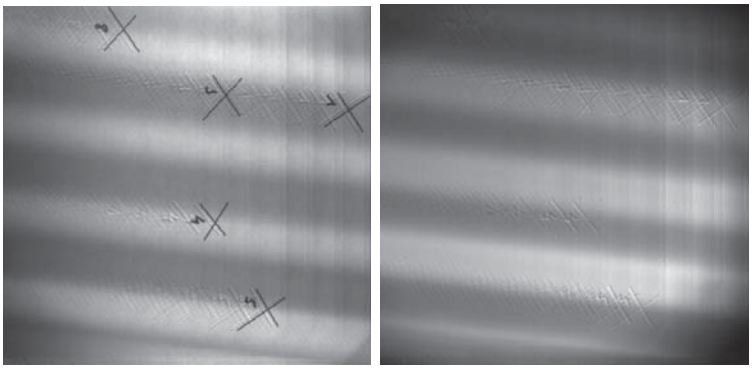

FIG. 14 – Results obtained on real images using four translated images (colinear vectors) : L(x,y) (left), V(x,y) (right)

Figure 16 shows $L(x, y)$ and $V(x, y)$ functions obtained with respectively with three, five, and eight translated images with un-colinear translation vectors. Using eight translated images gives quite good results even though « ghost effects »(pattern multiplications)

Author-produced version of the article published inJournal of Near Infrared Spectroscopy, 2008, 16, 4, 371-380.
The original publication is available at http://www.impublications.com/
doi: 10.1255/jnirs.809

appear on the resulting image (figure 17). This phenomenon is due to the insuffisant accuracy in the amplitude determination of the translation vectors. Indeed, we can observe the same effects on synthetic images when errors are introduced in each translations vectors (figure 18). The characteristics of induced error translation are listed Table 1 (small to large errors translation have been tested), with $\overline{\Delta_x}$ and $\overline{\Delta_y}$ respectively the mean error in the x and y direction translation (figure 15). Unfortunately, our imaging system plateform does not allow to apply many and accurate translations. It also does not make it possible to correctly spatially distribute the translations as we did with synthetic images.

	$\overline{\Delta_x}$	$\overline{\Delta_y}$
small errors	0.02	-0.015
medium errors	-0.115	0.155
large errors	-0.445	1.35

TAB. 1 – Charateristics of induced error translations

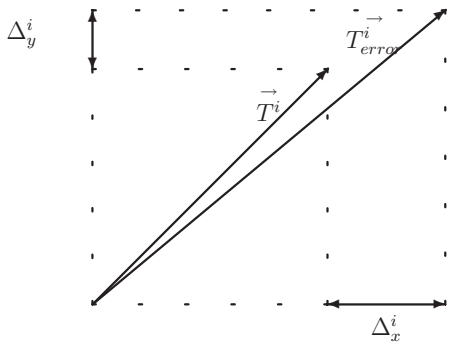

$$\overline{\Delta_x} = \frac{1}{N}\sum_{i=1}^{N}\Delta_x^i$$
$$\overline{\Delta_y} = \frac{1}{N}\sum_{i=1}^{N}\Delta_y^i$$

N=number of translations

FIG. 15 –Induced error translations

5 Conclusion

The objective of this study was to set up a methodology to separate the scene from the response of the hyperspectal imaging system. The method is based on imaging system

Original Image


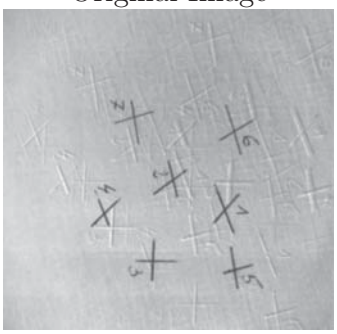


$L(x, y)$: Three translations, five translations and eight translations



$V(x, y)$: Three translations, five translations and eight translations

FIG. 16 – Results obtained on real images using 8 translated images (no-colinear vectors)

Author-produced version of the article published inJournal of Near Infrared Spectroscopy, 2008, 16, 4, 371-380.
The original publication is available at http://www.impublications.com/
doi: 10.1255/jnirs.809

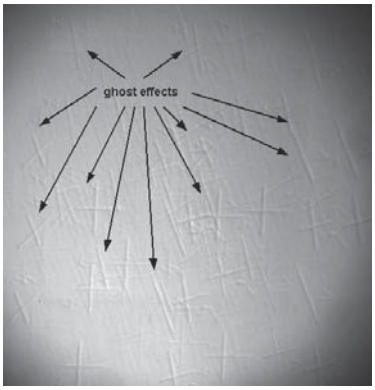

FIG. 17 – Ghost effects on resulting image $V(x, y)$

FIG. 18 – Ghost effects on resulting image $V(x, y)$ using synthetic images : errors effects on the translation vectors (slight errors (left), mean errors (center), large errors (right))

shifting followed by a Fourier Transform. The proposed method gives very good results on synthetic images using almost ten shifts. Although, some border effects due to low gray level on the image edges are visible. In real case, the results obtained with eight translated images are quite relevant. One of the main drawbacks of the method is its sensitivity to the translation determination accuracy, that can be reduces by using a more appropriate system to perform the translations (x-y table for exemple). Indeed, it is difficult to produce a high number of translated image and with spatial distribution of the translation vectors in the space as good as used in the case of synthetic images. However, this new method is an easy way for correcting images biaised by the imaging system reponse. It remains useable for any imaging system based on a CCD sensor.

Références

P. Geladi, J. Burger, and T. Lestander. Hyperspectral imaging : calibration problems and solutions. *Chemometrics and Intelligent Laboratory Systems*, 72 :209–217, 2004.

M. Grossberg and K. Nayar. What can be known about the radiometric response from images ? In *Proceedings of the 7th European Conference on Computer Vision-Part IV (ECCV '02)*, volume 2353, pages 189–205, London, UK, 2002. Springer-Verlag.

G. Healey. Radiometric ccd camera calibration and noise estimation. *IEEE Transalation on Pattern Analysis and Machine Intellelligence*, 16(3) :267–276, 1994.

B.K.P. Horn. *Robot Vision.* MIT Press, McGraw-Hill, 1986.

K.C. Lawrence, B. Park, W.R. Windham, and C. Mao. Calibration of pushbroom hyperspectral imaging system for agricultural inspection. *Transactions of ASAE*, 46(2) : 513–521, 2003.

R.C. Lyon, D.S. Lester, E.N. Lewis, E. Lee, L.X. Yu, E.H. Jefferson, and A.S. Hussain. Near infrared spectral imaging for quality assurance of pharmaceutical products : analysis of tablets to assess powder blend homogeneity. *APPS PharmSciTech*, 3(3) :1–15, 2002.

A. Mansouri, F.S. Marzani, and P. Gouton. Development of a protocol for ccd calibration : application to a multispectral imaging system. *International Journal of Robotics and Automation, Special Issue on Color Image Processing and Analysis for Machine Vision*, 20(2) :94–100., 2005.

G Polder and G. W. Van Der Heijden. Calibration and characterization of spectral imaging systems. In Q. Tong, Y. Zhu, and Z. Zhu, editors, *the Society of Photo-Optical Instrumentation Engineers (SPIE)*, volume 4548, pages 10–17. SPIE, 2001.

G. Polder, Van Der Heijden G. W., P. Keizera, and T. Ian. Calibration and characterisation of imaging spectrographs. *Journal of Near Infrared Spectroscopy*, 11 :193–210, 2003.

P.P. Tarel. Calibration radiométrique de caméra. Technical report, INRIA, Mars 1995 1995.

Y. Tsin, V. Ramesh, and T. Kanade. Statistical calibration of ccd imaging process. In *IEEE International Conference on Computer Vision (ICCV'01)*, 2001.

D. Van der Weken, M. Nachtegael, and E.E. Kerre. Using similarity measures and homogeneity for the comparison of images. *Image and Vision Computing*, 22(9) :695–702, 2004.

Y. Wonpil, C. Yunkoo, and S. Jung. Vignetting distortion correction method for high quality digital imaging. In *International conference on Pattern Recognition*, pages 666–669, Cambridge, UK, 2004.